

# GeoShield: Safeguarding Geolocation Privacy from Vision-Language Models via Adversarial Perturbations

Xinwei Liu<sup>1,2</sup>, Xiaojun Jia<sup>3\*</sup>, Yuan Xun<sup>1,2</sup>, Simeng Qin<sup>4</sup>, Xiaochun Cao<sup>5\*</sup>

<sup>1</sup>Institute of Information Engineering, CAS, Beijing, China

<sup>2</sup>School of Cyber Security, University of Chinese Academy of Sciences, Beijing, China

<sup>3</sup>Nanyang Technological University, Singapore

<sup>4</sup>Northeastern University, China

<sup>5</sup>School of Cyber Science and Technology, Shenzhen Campus of Sun Yat-sen University, Shenzhen, 518107, China  
 {liuxinwei,xunyuan}@iie.ac.cn, jiaxiaojunqaq@gmail.com, qinsimeng@neu.edu.cn, caoxiaochun@mail.sysu.edu.cn

## Abstract

Vision-Language Models (VLMs) such as GPT-4o now demonstrate a remarkable ability to infer users' locations from public shared images, posing a substantial risk to geoprivacy. Although adversarial perturbations offer a potential defense, current methods are ill-suited for this scenario: they often perform poorly on high-resolution images and low perturbation budgets, and may introduce irrelevant semantic content. To address these limitations, we propose **GeoShield**, a novel adversarial framework designed for robust geoprivacy protection in real-world scenarios. GeoShield comprises three key modules: a feature disentanglement module that separates geographical and non-geographical information, an exposure element identification module that pinpoints geo-revealing regions within an image, and a scale-adaptive enhancement module that jointly optimizes perturbations at both global and local levels to ensure effectiveness across resolutions. Extensive experiments on challenging benchmarks show that GeoShield consistently surpasses prior methods in black-box settings, achieving strong privacy protection with minimal impact on visual or semantic quality. To our knowledge, this work is the first to explore adversarial perturbations for defending against geolocation inference by advanced VLMs, providing a practical solution to escalating privacy concerns.

Code — <https://github.com/thinwayliu/Geoshield>

## Introduction

Recently, Vision-Language Models (VLMs) have emerged as a powerful paradigm that bridges computer vision and natural language processing (Alayrac et al. 2022; Yin et al. 2024; Liu et al. 2023b; Zhu et al. 2023). By jointly modeling visual and textual modalities, VLMs enable a wide range of capabilities, including image captioning (Li et al. 2024; Sarto, Cornia, and Cucchiara 2025), visual question answering (Kuang et al. 2025), and complex multimodal reasoning (Yang et al. 2023). Commercial large-scale VLMs (LVLMs), such as GPT-4, Claude 3.5, and Gemini 2.0, have seen widespread adoption due to their strong performance and versatility.

\*Correspondence to: Xiaojun Jia and Xiaochun Cao.  
 Copyright © 2026, Association for the Advancement of Artificial Intelligence (www.aaai.org). All rights reserved.

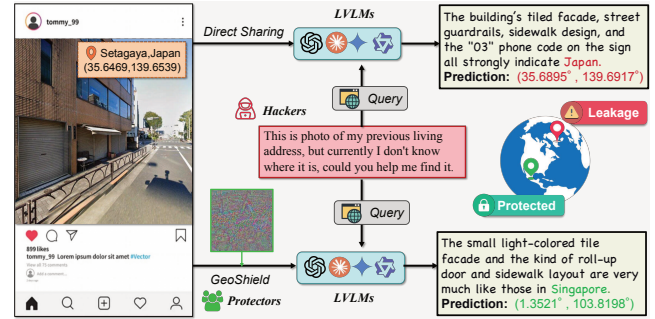
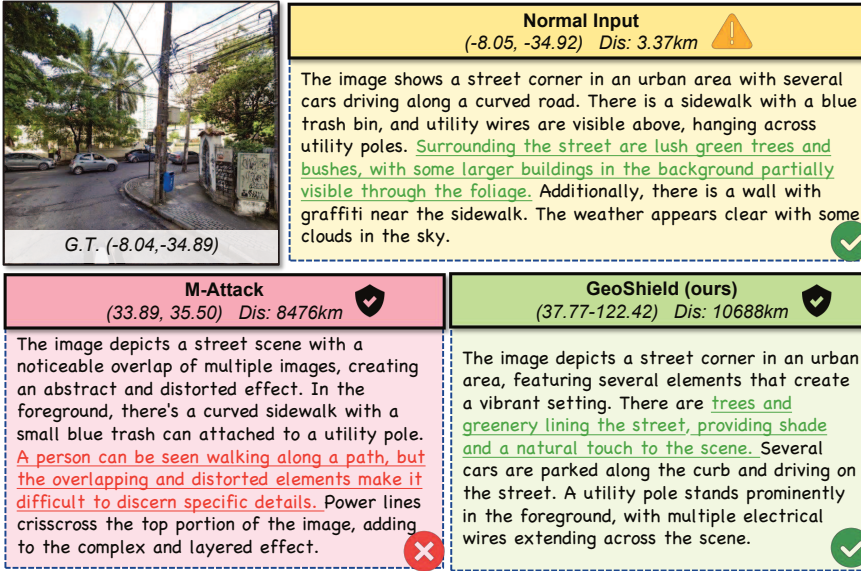


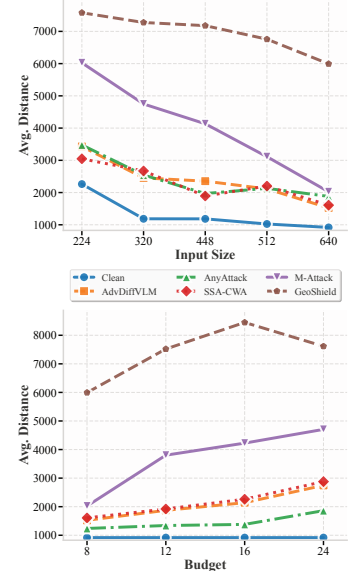
Figure 1: Public image sharing exposes users to geoprivacy threats, as LVLMs can accurately infer locations from visual content. GeoShield applies imperceptible perturbations to disrupt such inference and safeguard user privacy.

However, as the capabilities of VLMs continue to escalate, so do the associated privacy risks (Liang et al. 2022b; enhancing face obfuscation guided by semantic-aware attribution maps 2023; Guo et al. 2023; Dong et al. 2023a; Liang et al. 2024; Gong et al. 2024), particularly concerning geolocation inference (Mendes et al. 2024). Recent studies have highlighted the powerful geolocation abilities of these models (Luo et al. 2025; Zhang et al. 2025b; Jay et al. 2025): VLMs can not only recognize well-known landmarks, but also infer highly accurate geographic coordinates by analyzing subtle visual cues such as lighting conditions, vegetation, and architectural features. This level of inference closely mirrors the mechanics of GeoGuesser, where expert players deduce locations based on minimal information. The advent of VLMs has dramatically lowered the technical barriers for such inferences. For example, a photo casually shared on social media may be collected by malicious actors and queried using advanced VLMs to infer sensitive details, such as a user's home address, workplace, or frequent locations (see Fig. 1). Consequently, safeguarding geographic privacy while preserving the convenience and value of image sharing has become a pressing research challenge.

Recent studies have explored the use of adversarial perturbations (Liang, Wei, and Cao 2021; Liang et al. 2020,



(a) VLM responses and predictions on normal and protected inputs.



(b) Impact of input size and budget.

Figure 2: Comparison of semantic consistency and protection effectiveness under different methods: In (a), both methods offer protection, but M-attack introduces incorrect semantics while GeoShield preserves accurate descriptions; In (b), baseline performance declines with larger input size and smaller budget, while ours remains stable.

2022c,a; Wang et al. 2023; Liu et al. 2023a; Wang et al. 2025; Wei et al. 2018) as a means of defending against malicious AI models and applications (Van Le et al. 2023; Le et al. 2022; Liu et al. 2022). For geo-privacy protection, a practical strategy is to add carefully crafted adversarial perturbations to public images, thereby preventing unauthorized geolocation inference. However, conducting effective adversarial attacks against advanced commercial models remains challenging due to their closed-source nature. To address this issue, recent work (Zhang, Yi, and Sang 2022; Yin et al. 2023) has shown that integrating multiple white-box visual encoders and minimizing global feature distances between adversarial and target examples can significantly improve the transferability, thus enabling effective attacks against closed-source commercial models (Xu et al. 2024; Lu et al. 2023; Wei et al. 2023).

We systematically evaluated existing adversarial attacks for VLMs (AdvDiffVLM (Guo et al. 2024), AnyAttack (Zhang et al. 2025a), SSA-CWA (Dong et al. 2023b), M-Attack (Li et al. 2025)) for geographic protection. These methods manipulate perturbed image features to align with target images from different locations, misleading models to predict incorrect geolocations. However, our experiments reveal that all approaches face three major challenges.

Firstly, targeted attack methods are fundamentally incompatible with the objective of geo-privacy protection. While these attacks (e.g., M-Attack) aim to mislead VLMs into predicting incorrect locations by aligning image features with those of another image, they don't focus the features and regions within an image that might leak geographical information. Consequently, the generated perturbations often

fail to significantly reduce geo-localization accuracy. Moreover, by forcing feature alignment with an unrelated image, these methods not only offer suboptimal privacy protection but also distort the original content and introduce irrelevant semantic information, as illustrated in Fig. 2(a). Such modifications can degrade user experience and undermine other social applications, like content classification for recommendations on social media platforms.

Second, existing attacks typically generate low-resolution perturbations tailored to the input size of visual encoders (e.g., 224×224 for CLIP). Moreover, these methods are primarily evaluated on images with simple backgrounds and few objects, which makes them unsuitable for the high-resolution, object-rich images on social media. As Fig. 2(b) illustrates, upsampling these optimized low-resolution perturbations to higher-resolution images significantly degrades their effectiveness, and this protective effect diminishes even further as image resolution increases.

Third, the effectiveness of these attacks often depends on an excessively high perturbation budget (e.g., 16/255), which substantially degrades image quality. Fig. 2(b) further demonstrates that when the perturbation budget is constrained, existing methods generally fail to provide adequate geographic privacy protection.

To address these challenges, we propose GeoShield, a novel perturbation generation framework for real-world geo-privacy protection. GeoShield is designed to produce visually imperceptible yet highly effective perturbations that disrupt the geolocation capabilities of VLMs while preserving semantic integrity. It consists of three key modules: (1) Geographical and Non-Geographical Feature Disentanglement

(GNFD), which leverages VLMs to produce generic image descriptions and disentangle geographical features from general semantic features; (2) Geographical Exposure Element Identification (Geo-EE), which localizes geographical exposure elements (e.g., landmarks, architecture) using a combination of VLMs and object detection; and (3) Perturbation Scale Adaptive Enhancement (PSAE), which jointly optimizes perturbations over global and local patches to ensure effectiveness across varying image resolutions. These modules suppress geo-relevant features while preserving alignment with non-geographic semantics. Extensive experiments show that our method consistently outperforms existing methods under black-box settings.

Our contributions can be summarized as follows:

- We are the first to leverage adversarial perturbation to protect user geolocation privacy against powerful VLMs.
- We conduct a systematic evaluation of existing adversarial methods in the context of geo-privacy and reveal their limitations under realistic scenarios.
- We propose GeoShield, a novel framework that disentangles geo-relevant features, localizes geo-exposing regions, and enhances perturbation robustness across scale.
- Extensive experiments show that GeoShield consistently outperforms existing baselines under black-box conditions, achieving strong privacy protection with minimal semantic or visual degradation.

## Related Work

### Image Geo-Localization

Geolocation inference refers to the ability to determine precise geographic coordinates (latitude and longitude) from one or more input images (Clark et al. 2023; Vivanco Cepeda, Nayak, and Shah 2023). Traditionally, common localization approaches have relied on image-to-image retrieval techniques (Suresh, Chodosh, and Abello 2018; Wu and Huang 2022; Berton, Masone, and Caputo 2022). However, a significant limitation of these methods is the prohibitive requirement for large-scale global reference datasets, which renders them impractical for broad application. Another approach involves classification-based methods, where geographical maps are partitioned into discrete categories and models are trained to classify images into these predetermined regions (Theiner, Müller-Budack, and Ewerth 2022; Haas et al. 2024). Nevertheless, the generalization capabilities of these approaches remain constrained by fixed geographic granularity and the need for extensive annotated datasets tailored to each specific region.

Recent advancements in VLMs have demonstrated an unexpected proficiency in predicting geographic locations, despite not being explicitly trained for geolocation tasks (Wang et al. 2024; Zhang et al. 2024; Yang et al. 2024). Notably, Jay et al. (2025) conducted an evaluation of various open-source and closed-source VLMs for their precise geolocation capabilities, revealing surprisingly high accuracy. Furthermore, Luo et al. (2025) performed a study on the potential privacy risks associated with the visual reasoning capabilities of these models.

### Adversarial Attacks on VLMs

Adversarial attacks on VLMs aim to induce incorrect model outputs by adding imperceptible perturbations (Jia et al. 2025). Given that many commercial LVLMs are closed-source, black-box attacks—especially transfer-based attacks—are more practical. These transfer-based attacks generate adversarial examples on surrogate models such as CLIP (Radford et al. 2021) and BLIP (Li et al. 2022), which are then successfully transferred to target models. AttackVLM (Zhao et al. 2023) was the first to introduce this strategy, demonstrating that image-to-image feature matching achieves better transferability than image-to-text optimization. Subsequent approaches like CWA (Chen et al. 2023) and SSA-CWA (Dong et al. 2023b) have further enhanced transferability by leveraging ensemble surrogates and frequency-based transformations, showing notable success against commercial LVLMs such as Google Bard. Additionally, methods including AnyAttack (Zhang et al. 2025a) and AdvDiffVLM (Guo et al. 2024) incorporate self-supervised pretraining and diffusion guidance to generate transferable adversarial examples, albeit often at the expense of image quality or increased complexity. M-Attack (Li et al. 2025) further improves transfer success by introducing random cropping and resizing during optimization.

## Methodology

### Preliminary

Given a test geographical dataset  $D = \{(I_n, G_n)\}_{n=1}^N$ , where  $I_n$  denotes the  $n$ -th image and  $G_n = (\phi_n, \lambda_n)$  represents its true geographical coordinates (latitude and longitude), our core objective is to generate an imperceptible perturbation  $\delta_n$  for each image  $I_n$ . The resulting protected image  $I'_n = I_n + \delta_n$  is designed to mislead a target VLM, denoted as  $f_t$ , into predicting incorrect coordinates  $G'_n \neq G_n$ , thereby providing geographical privacy protection for users.

To quantify the effectiveness of protection, we compute the geolocation error as the great-circle distance (in kilometers) between the predicted and true coordinates. This error is calculated using the Haversine formula, which estimates the shortest distance over the Earth’s surface between two points. Given two locations with coordinates  $(\phi_1, \lambda_1)$  and  $(\phi_2, \lambda_2)$ , the distance  $d$  is computed as:

$$d = R \cdot \arctan 2 \left( \sqrt{\text{hav}(\theta)}, \sqrt{1 - \text{hav}(\theta)} \right), \quad (1)$$

where  $R$  is the Earth’s mean radius, and  $\theta$  is the central angle between the two points. The haversine of  $\theta$  is defined as:

$$\text{hav}(\theta) = \sin^2 \left( \frac{\Delta\phi}{2} \right) + \cos(\phi_1) \cdot \cos(\phi_2) \cdot \sin^2 \left( \frac{\Delta\lambda}{2} \right). \quad (2)$$

Our objective is to maximize the geographical distance between the predicted coordinates  $G'_n$  and the ground-truth coordinates  $G_n$ . This can be formulated as a constrained optimization problem:

$$\max_{\delta_n} d(f_t(I_n + \delta_n), G_n) \quad \text{s.t.} \quad \|\delta_n\|_\infty \leq \epsilon, \quad (3)$$

where  $\epsilon$  denotes the perturbation budget, constraining the magnitude of adversarial noise under the  $\ell_\infty$  norm.

In this work, we consider a black-box setting, where the protector has no access to the internal architecture, parameters, or training data of the target VLM. This aligns with realistic deployment scenarios, as privacy defenses are typically applied before the image is exposed to potential hackers. Moreover, commercial LVMs such as GPT-4o, Claude-3.5, and Gemini-2.5 are accessible only via APIs, making white-box, gradient-based geolocation attacks impractical.

## Limitations of Existing Baselines

Recent studies have shown that adversarial examples crafted using an ensemble of pre-trained image encoders exhibit significantly improved transferability and can successfully perform targeted attacks against commercial VLMs. Motivated by these findings, we adopt an ensemble-based strategy for geographic privacy protection. In the remainder of this paper, we assume both visual and textual encoders are implemented as ensembles of paired encoders, with each pair operating in a shared feature space. Given a protecting image  $x$  and a target image  $x_t$  sampled from a geographically distant location, our objective is to generate a targeted perturbation  $\delta$  such that the visual features of the perturbed image  $x + \delta$  are closely aligned with those of  $x_t$ . This can be formulated as the following constrained optimization problem:

$$\min_{\delta} \sum_{i=1}^M [\mathcal{S}(f_{\theta_i}(x + \delta), f_{\theta_i}(x_t))] \quad \text{s.t.} \quad \|\delta\|_{\infty} \leq \epsilon, \quad (4)$$

where  $f_{\theta_i}(\cdot)$  denotes the  $i$ -th image encoder in the ensemble and  $\mathcal{S}(\cdot, \cdot)$  is a feature-space similarity loss (e.g., cosine distance). However, applying existing attack baselines to solve the above problem encounters three significant challenges:

- Inconsistent Objective:** The primary goal of baseline methods is typically to mislead the model into classifying the perturbed image into a specific object or content. This differs from the goal of geographical privacy protection, which is to induce incorrect location predictions. As a result, these perturbations may not effectively reduce geolocation accuracy. Even though M-Attack reduces accuracy, it often severely distorts semantic features and introduces incorrect descriptions, as shown in Fig. 2 (a), thus compromising the usability of protected images in downstream applications.
- Low-Resolution Perturbations:** Most existing attack methods generate perturbations for low-resolution inputs (e.g.,  $224 \times 224$  for CLIP), and are evaluated on images with simple backgrounds and few objects. In practice, user-uploaded social media images are typically high-resolution and object-rich. Applying low-resolution noise to such images via upsampling will significantly reduce perturbation effectiveness. Fig. 2 (b) shows that baseline effectiveness declines rapidly as input size increases, especially for M-Attack.
- Excessive Budget:** To improve attack performance, baselines often adopt large perturbation budgets (e.g.,  $16/255$ ), leading to noticeable image quality degradation and poor user acceptance. However, as shown in Fig. 2

(b), baselines generally fail to maintain privacy protection under more realistic, lower-budget constraints.

## Our Proposed Method: GeoShield

To safeguard geo-privacy in high-resolution images while maintaining semantic integrity on a smaller perturbation budget, we introduce GeoShield, a novel framework comprises three core modules. The overall architecture of GeoShield is illustrated in Fig. 3.

**Geographical and Non-Geographical Feature Disentanglement (GNFD)** To effectively prevent VLMs from accurately inferring the geographic location from an image, it is essential to identify and suppress those directions in the visual features that encode geolocation information. At the same time, retaining features that are unrelated to geography ensures the preservation of the original semantic content. Here we introduce a feature decoupling mechanism. Specifically, we assume that an image representation  $\mathbf{z}$ , extracted by an ensemble of pre-trained image encoders, can be decomposed into two components: a geography-specific vector  $\mathbf{z}_{geo}$  and a non-geographic semantic vector  $\mathbf{z}_{non-geo}$ , formally expressed as

$$\mathbf{z} = \mathbf{z}_{geo} + \mathbf{z}_{non-geo}. \quad (5)$$

However, precisely disentangling geographical and non-geographical features in the feature space remains challenging, as most feature representations are inherently entangled and lack explicit annotations separating them. Thus, we employ an auxiliary VLM to implicitly approximate these components. Specifically, we design a tailored prompt for a powerful VLM (e.g., GPT-4o) to generate a detailed non-geographical textual description  $T_{non-geo}$  of the original image  $x$ , explicitly excluding any geographical clues such as place names, landmarks, or city/country identifiers (the exact prompt is provided in the appendix). This geo-filtered description is intended to capture the general semantic content of the image while omitting geographic information. We then encode  $T_{non-geo}$  using an ensemble of textual encoders  $g_{\theta_i}(\cdot)$ , aligned with those used for image feature extraction, to obtain the textual feature:

$$\mathbf{z}_{non-geo} \approx g_{\theta_i}(T_{non-geo}). \quad (6)$$

We regard  $\mathbf{z}_{non-geo}$  as the non-geographical feature component and use it to estimate the geographical features. Given a protecting image  $x$ , its visual feature can be denoted as  $f_{\theta_i}(x)$ . Therefore, we can approximate the geographical feature vector by subtracting  $\mathbf{z}_{non-geo}$  from the original feature. Formally, the geographical component  $\mathbf{z}_{geo}$  is given by:

$$\begin{aligned} \mathbf{z}_{geo} &= \mathbf{z} - \mathbf{z}_{non-geo} \\ &\approx f_{\theta_i}(x) - g_{\theta_i}(T_{non-geo}). \end{aligned} \quad (7)$$

**Geographical Exposure Element Identification (Geo-EE)** Disentangling geographical features solely at the global level is often insufficient to capture all the cues VLMs use for location prediction. Moreover, many reasoning-based models, such as o3, perform local recognition across different image regions before geographic localization. This highlights the need to identify local regions or visual elements that could expose geographical information.

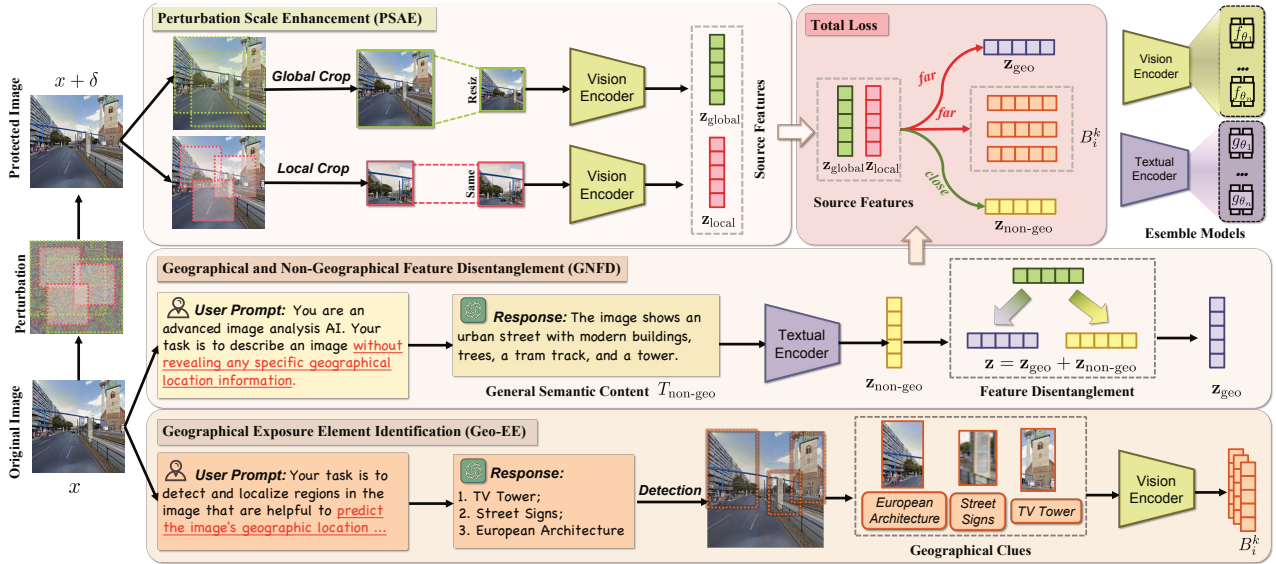


Figure 3: Overview of the GeoShield framework. GeoShield consists of three modules (GNFD, Geo-EE, and PSAE) that collaboratively suppress geographical cues while preserving semantic integrity in high-resolution images.

To address this, we introduce the Geographical Exposure Element Identification (Geo-EE) module. We again employ an auxiliary VLM to identify and generate the names of objects or landmarks within the image that may reveal geographic information, such as “European Architecture” or “TV Tower.” These entities are assumed to be strongly associated with specific locations. We then use these names as prompts for a pre-trained object detection model (e.g., GroundingDINO (Liu et al. 2023c) or SAM (Kirillov et al. 2023)) to identify and output a set of local geo-indicative bounding boxes, denoted as  $\mathcal{B} = \{b_1, b_2, \dots, b_K\}$ . For each box  $b_k$ , we crop the corresponding image region  $x_{b_k}$  and extract visual features using the same ensemble of image encoders  $f_{\theta_i}(\cdot)$  as in the GNFD module. Formally, the feature extracted from the  $i$ -th encoder for the  $k$ -th bounding box is:

$$B_i^k = f_{\theta_i}(x_{b_k}) \quad (8)$$

These local features  $B_i^k$  approximate subsets of the geographical information present in the original image. By isolating such fine-grained cues, we enable more comprehensive protection of geographical privacy.

**Perturbation Scale Enhancement** Through the GNFD and Geo-EE modules, we extract approximate geographical features ( $\mathbf{z}_{\text{geo}}, B_i^k$ ) and non-geographical features ( $\mathbf{z}_{\text{non-geo}}$ ) from an image. However, as previously discussed, perturbations often struggle with scale adaptability on high-resolution images, leading to diminished privacy protection.

Therefore, we propose the Perturbation Scale Adaptive Enhancement (PSAE) module, which employs a joint global and local optimization. We first follow the data augmentation strategy from M-Attack by applying random cropping to the entire image before encoding, which has been shown to significantly improve transferability. Specifically, in each iteration, we perform random cropping on the entire image

$x$  to obtain global source features  $f_{\text{global}}$ . In addition, we simultaneously reinforce perturbations in randomly sampled local regions, each matching the input size of the visual encoders (for example,  $224 \times 224$  for  $x_{\text{patch},t}$ ), and encode these regions to yield a set of local source features  $\{f_{\text{local},t}\}_{t=1}^{N_{\text{patch}}}$ . We aggregate these local features by averaging over all sampled patches, resulting in the following formulation:

$$f_{\theta_i}^{\text{local}} = \frac{1}{N_{\text{patch}}} \sum_{t=1}^{N_{\text{patch}}} f_{\theta_i}(x_{\text{patch},t}). \quad (9)$$

By jointly optimizing both  $f_{\text{global}}$  and  $\{f_{\text{local},t}\}$  in a multi-scale manner, PSAE preserves fine-grained details and enables locally refined updates based on the global perturbation. In particular, to further enhance transferability through increased randomness, we use the global source features  $f_{\text{global}}$  obtained in each iteration as the decomposition targets  $f_{\theta_i}(x)$  in the GNFD module.

**Total Loss Function:** Based on the extracted features, we construct the following loss. The primary objective is to minimize the similarity between the source global and local features of the perturbed image and the geographical features, while maximizing similarity with non-geographical semantic features to preserve semantic integrity. This objective can be formalized as the following problem:

$$\begin{aligned} \min_{\delta} \sum_{i=1}^N & \left\{ [\mathcal{S}(f_{\theta_i}^{\text{global}}(x'), \mathbf{z}_{\text{geo}}) + \mathcal{S}(f_{\theta_i}^{\text{local}}(x'), \mathbf{z}_{\text{geo}})] \right. \\ & + \alpha \sum_{k=1}^K [\mathcal{S}(f_{\theta_i}^{\text{global}}(x'), B_i^k) + \mathcal{S}(f_{\theta_i}^{\text{local}}(x'), B_i^k)] \\ & \left. - \beta [\mathcal{S}(f_{\theta_i}^{\text{global}}(x'), \mathbf{z}_{\text{non-geo}}) + \mathcal{S}(f_{\theta_i}^{\text{local}}(x'), \mathbf{z}_{\text{non-geo}})] \right\} \\ \text{s.t. } & \|\delta\|_{\infty} \leq \epsilon \end{aligned}$$

Dataset	Model	GPT-4o					GPT-4.1					Claude-3.5					Gemini-2.5				
		1km	25km	200km	750km	2500km	1km	25km	200km	750km	2500km	1km	25km	200km	750km	2500km	1km	25km	200km	750km	2500km
Google Street View	Clean	7.3	17.7	41.6	73.4	90.6	9.1	23.2	48.5	78.0	92.8	4.9	9.0	27.5	57.8	78.1	8.7	21.9	47.6	79.2	93.5
	RN	6.9	16.1	40.6	73.2	90.7	9.6	23.7	48.8	77.5	92.3	4.7	8.9	27.2	56.4	77.8	8.9	21.2	47.1	80.3	92.5
	AdvDiffVLM	5.5	13.4	34.2	68.0	87.0	7.7	20.0	43.4	74.4	90.3	2.7	8.4	24.8	53.9	73.8	8.1	20.4	45.6	77.8	93.0
	AnyAttack	6.2	15.9	37.7	68.7	87.3	7.9	20.4	44.4	73.1	89.5	2.8	8.4	24.1	51.4	74.2	8.0	19.8	44.2	77.3	91.2
	SSA-CWA	4.7	12.1	31.8	62.9	83.4	7.2	18.4	40.8	70.0	88.3	1.4	6.1	18.3	44.9	62.1	7.2	18.8	40.6	74.5	90.5
	M-Attack	3.3	9.1	24.5	48.7	71.1	4.9	12.6	30.3	54.9	76.1	1.4	5.3	15.3	35.8	56.3	6.1	16.7	37.6	66.8	86.3
	GeoShield	<b>1.1</b>	<b>2.9</b>	<b>7.6</b>	<b>17.5</b>	<b>33.8</b>	<b>1.4</b>	<b>3.6</b>	<b>9.1</b>	<b>20.9</b>	<b>37.9</b>	<b>0.1</b>	<b>1.1</b>	<b>5.2</b>	<b>12.5</b>	<b>27.4</b>	<b>4.7</b>	<b>13.0</b>	<b>32.4</b>	<b>59.1</b>	<b>80.9</b>
Img2gps	Clean	14.4	38.9	55.8	71.4	84.6	18.2	46.3	59.4	73.9	87.4	9.1	30.0	43.4	61.9	77.1	18.2	45.5	59.7	74.9	86.4
	RN	14.1	38.8	55.1	70.7	84.7	17.8	44.9	58.9	73.3	85.6	8.6	28.9	42.1	60.5	76.9	18.0	45.4	58.9	73.2	86.0
	AdvDiffVLM	13.8	35.7	49.9	67.4	82.3	17.3	43.5	56.8	70.0	83.1	8.3	26.7	41.4	58.2	74.5	17.8	43.2	56.8	70.1	82.1
	AnyAttack	14.0	36.9	52.1	67.1	81.4	17.4	43.3	56.6	71.5	84.3	8.2	26.5	40.0	57.8	74.3	17.8	40.8	56.5	69.4	81.6
	SSA-CWA	13.5	33.1	47.2	64.7	76.8	15.9	39.8	53.0	67.2	81.3	7.4	24.3	35.1	52.0	69.3	16.1	39.6	53.6	68.5	78.4
	M-Attack	9.2	23.0	32.9	46.2	61.1	13.2	30.1	40.0	50.5	65.3	5.6	16.9	24.1	36.4	52.8	15.2	36.6	49.3	61.6	77.3
	GeoShield	<b>4.0</b>	<b>9.7</b>	<b>12.3</b>	<b>20.0</b>	<b>5.8</b>	<b>9.2</b>	<b>13.2</b>	<b>16.2</b>	<b>23.2</b>	<b>38.3</b>	<b>2.4</b>	<b>6.7</b>	<b>8.6</b>	<b>14.6</b>	<b>30.1</b>	<b>10.4</b>	<b>25.4</b>	<b>31.8</b>	<b>41.7</b>	<b>55.3</b>

Table 1: Geolocation prediction accuracy (%) at multiple distance levels on Google Street View and Im2GPS3k datasets. GeoShield consistently provides superior geoprivacy protection compared to existing baselines across all black-box VLMs.

where  $x' = x + \delta$  is the perturbed image,  $f_{\theta_i}(\cdot)$  denotes the  $i$ -th visual encoder in the ensemble, and  $\mathcal{S}(\cdot, \cdot)$  indicates cosine similarity.  $\alpha$  and  $\beta$  are weighting coefficients.

This optimization can be addressed using standard adversarial frameworks such as I-FGSM (Kurakin, Goodfellow, and Bengio 2018), PGD (Madry et al. 2017), or C&W (Carlini and Wagner 2017). Following M-Attack, we adopt a uniformly weighted ensemble with I-FGSM. Full algorithmic details are provided in the appendix.

## Experiment

### Experimental Settings

**Datasets.** We conducted experiments on two public geographic image datasets: Google Street View and Im2GPS3k, both of which provide images paired with GPS coordinates. The Google Street View dataset contains 1,602 images from 1,563 unique cities across 88 countries. The Im2GPS3k dataset includes approximately 3,000 geotagged images from sources such as Flickr. Unless otherwise specified, all images were resized to  $640 \times 640$  pixels. In addition, target images for baseline methods were randomly selected from MSCOCO dataset (Lin et al. 2014).

**Implementation Settings.** For fair comparison and consistency with prior work, we used three CLIP variants (ViT-B/16, ViT-B/32, and ViT-g-14-laion2B-s12B-b42K) as surrogate models to generate perturbations. The budget was set to 8/255 under the  $\ell_\infty$  norm to avoid visual degradation, with an attack step size of 1/255 and 200 attack iterations. Main results are reported on four popular black-box VLMs: GPT-4o, GPT-4.1, Claude-3.5, and Gemini-2.5; Unless otherwise specified, we default to using GPT-4o as both the auxiliary and target VLM for all experiments, and they were conducted on four NVIDIA A100 GPUs (80GB).

**Evaluation Metrics.** Geolocation accuracy was measured by the Haversine distance between predicted and ground truth coordinates, evaluated at five granularities: street (1 km), city (25 km), region (200 km), country (750 km), and continent (2,500 km). For some experiments, average distance was also reported. To assess semantic preservation, we used VLMs to generate textual descriptions for both original and perturbed images, and measured semantic similarity using BLEU, ROUGE, and BERTScore (BERT-S).



Figure 4: Visualization of different protected images.

Budget $\epsilon$	Method	Llava-1.5			GPT-4o		
		BLEU	ROUGE	BERT-S	BLEU	ROUGE	BERT-S
8/255	AdvDiffVLM	0.50	0.62	0.95	0.14	0.31	0.90
	AnyAttack	0.48	0.59	0.94	0.13	0.31	0.90
	SSA-CWA	0.45	0.57	0.93	0.13	0.31	0.90
	M-Attack	0.22	0.39	0.91	0.09	0.26	0.88
	GeoShield	0.25	0.41	0.92	0.11	0.29	0.89
16/255	AdvDiffVLM	0.48	0.59	0.94	0.12	0.29	0.89
	AnyAttack	0.43	0.55	0.94	0.12	0.30	0.90
	SSA-CWA	0.32	0.47	0.92	0.11	0.29	0.89
	M-Attack	0.15	0.34	0.89	0.07	0.24	0.87
	GeoShield	0.20	0.37	0.91	0.09	0.26	0.89

Table 2: Semantic similarity metrics between original and protected images evaluated on Llava-1.5 and GPT-4o.

### Comparative Results

**Effectiveness.** We evaluate the protection effectiveness of GeoShield by measuring the geolocation accuracy of four commercial VLMs. In Tab. 1, GeoShield consistently achieves the lowest localization accuracy across all models and datasets, significantly outperforming baselines such as M-Attack and SSA-CWA. For instance, on the Google Street View dataset, GeoShield reduces the 1 km-level accuracy from 7.3% (clean) to 1.1% on GPT-4o, and from 4.9% to just 0.1% on Claude-3.5. These confirm effectiveness and transferability of GeoShield under black-box settings.

Fig. 2(b) further illustrates the impact of input resolution and perturbation budget on protection performance. As input size increases from 224 to 640, the effectiveness of base-

Metric	Effectiveness (Avg. Dis)			Semantic Consistency		
	GPT-4o	GPT-4.1	O1	BLEU	ROUGE	BERT-S
w/o Geo-EE	7046	6578	5840	0.1067	0.2855	0.8937
w/o GNFD	4481	4229	4307	0.1026	0.2915	0.8945
w/o PSAE	4932	4261	4629	0.1071	0.2918	0.8954
All losses	<b>7564</b>	<b>6868</b>	<b>6780</b>	<b>0.1078</b>	<b>0.2923</b>	<b>0.8986</b>

Table 3: Ablation results for GeoShield on geoprivacy protection and semantic consistency. Each module is essential for strong protection and content preservation.

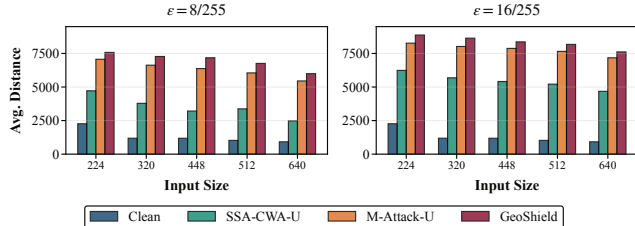


Figure 5: Average distance under untargeted attacks for two perturbation budgets.

line methods drops sharply, whereas GeoShield consistently maintains high protection efficacy. Moreover, ours remains robust even under smaller perturbation budgets  $\epsilon = 8$ , underscoring its practicality for real-world scenarios.

**Semantic Preservation.** We further evaluate the semantic consistency between the original and protected images, as shown in Table 2. While GeoShield does not always achieve the highest semantic consistency among all methods, previous effectiveness experiments indicate that, except for M-Attack, other baselines fail to provide an effective protection. For a fair comparison, we argue that a good protection method must first ensure geoprivacy effectiveness before considering semantic consistency. Focusing on the most competitive baseline, we observe that GeoShield consistently achieves higher semantic consistency scores than M-Attack. This illustrates that our perturbations can protect geoprivacy without sacrificing the core semantic content of the image, which is also consistent with the qualitative examples in Fig. 2 (a). Even under a stronger perturbation budget, GeoShield maintains better semantic preservation than M-Attack, supporting practical application for safe image sharing on social media.

**Visualization.** Fig. 4 shows examples of perturbed images from GeoShield and baselines. GeoShield maintains high visual quality with less artifacts, while methods like Any-Attack and SSA-CWA introduce more visible noise. Moreover, unlike methods that align perturbations to target image, ours avoids semantically misleading distortions, thus better maintaining content authenticity. Additional visualizations and perturbation heatmaps are provided in the appendix.

## Discussion

**Ablation Study.** An ablation study (Tab. 3) demonstrates that removing any GeoShield module results in noticeable performance degradation. Disabling Geo-EE signif-

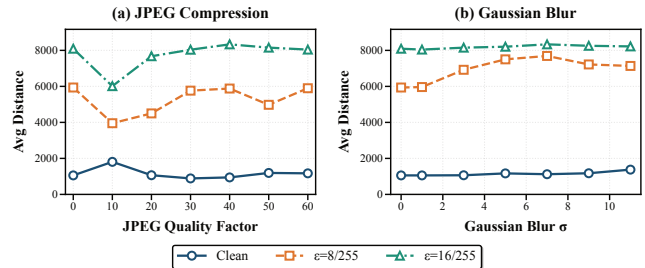


Figure 6: GeoShield maintains geoprivacy protection across varying levels of JPEG compression and Gaussian blur.

icantly weakens the framework’s ability to localize geo-sensitive regions, leading to reduced protection, particularly for reasoning-based models like o1. Excluding PSAE also causes a marked decline in effectiveness, which results the robustness across varying image resolutions. Most notably, omitting GNFD leads to the greatest decrease in both geoprivacy protection and semantic consistency, underscoring the central role of feature disentanglement. These findings confirm that all three modules are indispensable for robust and reliable geoprivacy protection.

**Untargeted Attack Baselines.** Previous sections primarily presented results for baselines under targeted attack settings. Here, we further evaluate the untargeted attack performance of SSA-CWA and M-Attack (denoted as SSA-CWA-U and M-Attack-U). As shown in Fig. 5, M-Attack-U achieves better protection than SSA-CWA-U, but its effectiveness consistently lags behind that of GeoShield across both perturbation budgets. We speculate that the effectiveness of M-Attack-U may be due to its loss to push features away from the original image representation, which inadvertently suppresses geographical cues, which is partially consistent with ours. Overall, GeoShield provides the most robust geoprivacy protection across all evaluated settings.

**Robustness to Transformation.** We evaluate the robustness of GeoShield against common image transformations, specifically JPEG compression and Gaussian blur, which frequently occur in real-world image sharing. As shown in Fig. 6, GeoShield consistently provides strong geoprivacy protection across a broad range of JPEG quality factors and blur radii. Even under heavy compression or blurring, the geolocation error remains substantially higher than the clean baseline. These results demonstrate the practical robustness of GeoShield for real-world deployment.

## Conclusion

We presented GeoShield, a novel framework for protecting geolocation privacy in VLMs. Extensive experiments demonstrate that GeoShield effectively prevents accurate geolocation inference while preserving both semantic integrity and image usability. Its robust and scalable design makes it a practical solution for applications where geoprivacy is critical. Our work not only offers a promising direction for geographic privacy defense, but also provides insights that can be extended to broader privacy protection tasks.

## Acknowledgments

This research is supported by Shenzhen Science and Technology Program (No.KQTD20221101093559018); by the National Natural Science Foundation of China (No.62025604); by Ningbo Science and Technology Innovation 2025 Major Project (2025Z027); by the Open Topics from the Lion Rock Labs of Cyberspace Security (under the project #LRL24009); by the National Research Foundation, Singapore, and DSO National Laboratories under the AI Singapore Programme (AISG Award No: AISG4-GC-2023-008-1B); by the National Research Foundation Singapore and the Cyber Security Agency under the National Cybersecurity R&D Programme (NCRP25-P04-TAICeN); and by the Prime Minister's Office, Singapore under the Campus for Research Excellence and Technological Enterprise (CREATE) Programme. Any opinions, findings and conclusions, or recommendations expressed in these materials are those of the author(s) and do not reflect the views of the National Research Foundation, Singapore, Cyber Security Agency of Singapore, Singapore.

## References

Alayrac, J.-B.; Donahue, J.; Luc, P.; Miech, A.; Barr, I.; Hasson, Y.; Lenc, K.; Mensch, A.; Millican, K.; Reynolds, M.; et al. 2022. Flamingo: a visual language model for few-shot learning. *NeurIPS*, 35: 23716–23736.

Bertoni, G.; Masone, C.; and Caputo, B. 2022. Rethinking visual geo-localization for large-scale applications. In *CVPR*.

Carlini, N.; and Wagner, D. 2017. Towards evaluating the robustness of neural networks. In *2017 ieee symposium on security and privacy (sp)*, 39–57. Ieee.

Chen, H.; Zhang, Y.; Dong, Y.; Yang, X.; Su, H.; and Zhu, J. 2023. Rethinking model ensemble in transfer-based adversarial attacks. *arXiv preprint arXiv:2303.09105*.

Clark, B.; Kerrigan, A.; Kulkarni, P. P.; Cepeda, V. V.; and Shah, M. 2023. Where we are and what we're looking at: Query based worldwide image geo-localization using hierarchies and scenes. In *CVPR*.

Dong, X.; Wang, R.; Liang, S.; Liu, A.; and Jing, L. 2023a. Face Encryption via Frequency-Restricted Identity-Agnostic Attacks. In *ACM MM*.

Dong, Y.; Chen, H.; Chen, J.; Fang, Z.; Yang, X.; Zhang, Y.; Tian, Y.; Su, H.; and Zhu, J. 2023b. How robust is google's bard to adversarial image attacks? *arXiv preprint arXiv:2309.11751*.

enhancing face obfuscation guided by semantic-aware attribution maps, P. 2023. Privacy-enhancing face obfuscation guided by semantic-aware attribution maps. *TIFS*.

Gong, J.; Cai, W.; Liang, S.; Guan, Z.; Wang, T.; and Chang, E.-C. 2024. WFCAT: Augmenting Website Fingerprinting with Channel-wise Attention on Timing Features. *arXiv preprint arXiv:2412.11487*.

Guo, J.; Zheng, X.; Liu, A.; Liang, S.; Xiao, Y.; Wu, Y.; and Liu, X. 2023. Isolation and Induction: Training Robust Deep Neural Networks against Model Stealing Attacks. In *ACM MM*.

Guo, Q.; Pang, S.; Jia, X.; Liu, Y.; and Guo, Q. 2024. Efficient generation of targeted and transferable adversarial examples for vision-language models via diffusion models. *TIFS*.

Haas, L.; Skreta, M.; Alberti, S.; and Finn, C. 2024. Pigeon: Predicting image geolocations. In *CVPR*.

Jay, N.; Nguyen, H. M.; Hoang, T. D.; and Haimes, J. 2025. Evaluating precise geolocation inference capabilities of vision language models. *arXiv preprint arXiv:2502.14412*.

Jia, X.; Gao, S.; Qin, S.; Pang, T.; Du, C.; Huang, Y.; Li, X.; Li, Y.; Li, B.; and Liu, Y. 2025. Adversarial Attacks against Closed-Source MLLMs via Feature Optimal Alignment. *arXiv preprint arXiv:2505.21494*.

Kirillov, A.; Mintun, E.; Ravi, N.; Mao, H.; Rolland, C.; Gustafson, L.; Xiao, T.; Whitehead, S.; Berg, A. C.; Lo, W.-Y.; Dollár, P.; and Girshick, R. 2023. Segment Anything. *arXiv:2304.02643*.

Kuang, J.; Shen, Y.; Xie, J.; Luo, H.; Xu, Z.; Li, R.; Li, Y.; Cheng, X.; Lin, X.; and Han, Y. 2025. Natural language understanding and inference with mllm in visual question answering: A survey. *ACM Computing Surveys*, 57(8): 1–36.

Kurakin, A.; Goodfellow, I. J.; and Bengio, S. 2018. Adversarial examples in the physical world. In *Artificial intelligence safety and security*, 99–112. Chapman and Hall/CRC.

Le, T.-N.; Gu, T.; Nguyen, H. H.; and Echizen, I. 2022. Rethinking Adversarial Examples for Location Privacy Protection. In *2022 IEEE International Workshop on Information Forensics and Security (WIFS)*, 1–6. IEEE.

Li, J.; Li, D.; Xiong, C.; and Hoi, S. 2022. Blip: Bootstrapping language-image pre-training for unified vision-language understanding and generation. In *ICML*.

Li, W.; Fan, H.; Wong, Y.; Yang, Y.; and Kankanhalli, M. 2024. Improving context understanding in multimodal large language models via multimodal composition learning. In *ICML*.

Li, Z.; Zhao, X.; Wu, D.-D.; Cui, J.; and Shen, Z. 2025. A frustratingly simple yet highly effective attack baseline: Over 90% success rate against the strong black-box models of gpt-4.5/4o/01. *arXiv preprint arXiv:2503.10635*.

Liang, S.; Gong, J.; Fang, T.; Liu, A.; Wang, T.; Liu, X.; Cao, X.; Tao, D.; and Ee-Chien, C. 2024. Red Pill and Blue Pill: Controllable Website Fingerprinting Defense via Dynamic Backdoor Learning. *arXiv preprint arXiv:2412.11471*.

Liang, S.; Li, L.; Fan, Y.; Jia, X.; Li, J.; Wu, B.; and Cao, X. 2022a. A large-scale multiple-objective method for black-box attack against object detection. In *ECCV*.

Liang, S.; Liu, A.; Liang, J.; Li, L.; Bai, Y.; and Cao, X. 2022b. Imitated detectors: Stealing knowledge of black-box object detectors. In *ACM MM*.

Liang, S.; Wei, X.; and Cao, X. 2021. Generate more imperceptible adversarial examples for object detection. In *ICML 2021 Workshop on Adversarial Machine Learning*.

Liang, S.; Wei, X.; Yao, S.; and Cao, X. 2020. Efficient adversarial attacks for visual object tracking. In *ECCV*.

Liang, S.; Wu, B.; Fan, Y.; Wei, X.; and Cao, X. 2022c. Parallel rectangle flip attack: A query-based black-box attack against object detection. *arXiv preprint arXiv:2201.08970*.

Lin, T.-Y.; Maire, M.; Belongie, S.; Hays, J.; Perona, P.; Ramanan, D.; Dollár, P.; and Zitnick, C. L. 2014. Microsoft coco: Common objects in context. In *ECCV*.

Liu, A.; Guo, J.; Wang, J.; Liang, S.; Tao, R.; Zhou, W.; Liu, C.; Liu, X.; and Tao, D. 2023a. {X-Adv}: Physical adversarial object attacks against x-ray prohibited item detection. In *32nd USENIX Security Symposium (USENIX Security 23)*.

Liu, H.; Li, C.; Wu, Q.; and Lee, Y. J. 2023b. Visual instruction tuning. *NeurIPS*, 36: 34892–34916.

Liu, S.; Zeng, Z.; Ren, T.; Li, F.; Zhang, H.; Yang, J.; Li, C.; Yang, J.; Su, H.; Zhu, J.; et al. 2023c. Grounding dino: Marrying dino with grounded pre-training for open-set object detection. *arXiv preprint arXiv:2303.05499*.

Liu, X.; Liu, J.; Bai, Y.; Gu, J.; Chen, T.; Jia, X.; and Cao, X. 2022. Watermark vaccine: Adversarial attacks to prevent watermark removal. In *ECCV*. Springer.

Lu, D.; Wang, Z.; Wang, T.; Guan, W.; Gao, H.; and Zheng, F. 2023. Set-level guidance attack: Boosting adversarial transferability of vision-language pre-training models. In *ICCV*.

Luo, W.; Lu, T.; Zhang, Q.; Liu, X.; Hu, B.; Zhao, Y.; Zhao, J.; Gao, S.; McDaniel, P.; Xiang, Z.; et al. 2025. Doxing via the Lens: Revealing Location-related Privacy Leakage on Multi-modal Large Reasoning Models. *arXiv preprint arXiv:2504.19373*.

Madry, A.; Makelov, A.; Schmidt, L.; Tsipras, D.; and Vladu, A. 2017. Towards deep learning models resistant to adversarial attacks. *arXiv preprint arXiv:1706.06083*.

Mendes, E.; Chen, Y.; Hays, J.; Das, S.; Xu, W.; and Ritter, A. 2024. Granular privacy control for geolocation with vision language models. *arXiv preprint arXiv:2407.04952*.

Radford, A.; Kim, J. W.; Hallacy, C.; Ramesh, A.; Goh, G.; Agarwal, S.; Sastry, G.; Askell, A.; Mishkin, P.; Clark, J.; et al. 2021. Learning transferable visual models from natural language supervision. In *ICML*.

Sarto, S.; Cornia, M.; and Cucchiara, R. 2025. Image captioning evaluation in the age of multimodal llms: Challenges and future perspectives. *arXiv preprint arXiv:2503.14604*.

Suresh, S.; Chodosh, N.; and Abello, M. 2018. Deepgeo: Photo localization with deep neural network. *arXiv preprint arXiv:1810.03077*.

Theiner, J.; Müller-Budack, E.; and Ewerth, R. 2022. Interpretable semantic photo geolocation. In *WACV*.

Van Le, T.; Phung, H.; Nguyen, T. H.; Dao, Q.; Tran, N. N.; and Tran, A. 2023. Anti-dreambooth: Protecting users from personalized text-to-image synthesis. In *ICCV*.

Vivanco Cepeda, V.; Nayak, G. K.; and Shah, M. 2023. Geo-clip: Clip-inspired alignment between locations and images for effective worldwide geo-localization. *NeurIPS*.

Wang, L.; Zhang, T.; Qu, Y.; Liang, S.; Chen, Y.; Liu, A.; Liu, X.; and Tao, D. 2025. Black-Box Adversarial Attack on Vision Language Models for Autonomous Driving. *arXiv preprint arXiv:2501.13563*.

Wang, Z.; Xu, D.; Khan, R. M. S.; Lin, Y.; Fan, Z.; and Zhu, X. 2024. Llmgeo: Benchmarking large language models on image geolocation in-the-wild. *arXiv preprint arXiv:2405.20363*.

Wang, Z.; Zhang, Z.; Liang, S.; and Wang, X. 2023. Diversifying the High-level Features for better Adversarial Transferability. *arXiv preprint arXiv:2304.10136*.

Wei, X.; Liang, S.; Chen, N.; and Cao, X. 2018. Transferable adversarial attacks for image and video object detection. *arXiv preprint arXiv:1811.12641*.

Wei, Z.; Chen, J.; Wu, Z.; and Jiang, Y.-G. 2023. Enhancing the self-universality for transferable targeted attacks. In *CVPR*.

Wu, M.; and Huang, Q. 2022. Im2city: image geolocation via multi-modal learning. In *Proceedings of the 5th ACM SIGSPATIAL International Workshop on AI for Geographic Knowledge Discovery*, 50–61.

Xu, W.; Chen, K.; Gao, Z.; Wei, Z.; Chen, J.; and Jiang, Y.-G. 2024. Highly transferable diffusion-based unrestricted adversarial attack on pre-trained vision-language models. In *ACM MM*.

Yang, Y.; Wang, S.; Li, D.; Sun, S.; and Wu, Q. 2024. GeoLocator: A location-integrated large multimodal model (LMM) for inferring geo-privacy. *Applied Sciences*, 14(16): 7091.

Yang, Z.; Li, L.; Wang, J.; Lin, K.; Azarnasab, E.; Ahmed, F.; Liu, Z.; Liu, C.; Zeng, M.; and Wang, L. 2023. Mm-react: Prompting chatgpt for multimodal reasoning and action. *arXiv preprint arXiv:2303.11381*.

Yin, S.; Fu, C.; Zhao, S.; Li, K.; Sun, X.; Xu, T.; and Chen, E. 2024. A survey on multimodal large language models. *National Science Review*, nwae403.

Yin, Z.; Ye, M.; Zhang, T.; Du, T.; Zhu, J.; Liu, H.; Chen, J.; Wang, T.; and Ma, F. 2023. Vlattack: Multimodal adversarial attacks on vision-language tasks via pre-trained models. *NeurIPS*.

Zhang, G.; Zhang, Y.; Zhang, K.; and Tresp, V. 2024. Can vision-language models be a good guesser? exploring vlms for times and location reasoning. In *WACV*.

Zhang, J.; Ye, J.; Ma, X.; Li, Y.; Yang, Y.; Chen, Y.; Sang, J.; and Yeung, D.-Y. 2025a. AnyAttack: Towards Large-scale Self-supervised Adversarial Attacks on Vision-language Models. In *CVPR*.

Zhang, J.; Yi, Q.; and Sang, J. 2022. Towards adversarial attack on vision-language pre-training models. In *ACM MM*.

Zhang, Z.; Li, R.; Kabir, T.; and Boyd-Graber, J. 2025b. Navig: Natural language-guided analysis with vision language models for image geo-localization. *arXiv preprint arXiv:2502.14638*.

Zhao, Y.; Pang, T.; Du, C.; Yang, X.; Li, C.; Cheung, N.-M. M.; and Lin, M. 2023. On evaluating adversarial robustness of large vision-language models. *NeurIPS*.

Zhu, D.; Chen, J.; Shen, X.; Li, X.; and Elhoseiny, M. 2023. Minigpt-4: Enhancing vision-language understanding with advanced large language models. *arXiv preprint arXiv:2304.10592*.

## A Detailed Description of GeoShield

This section provides a comprehensive algorithmic description of our proposed GeoShield framework, detailing the implementation specifics and operational flow of each core module. Algorithm 1 presents the complete procedure for generating geographical privacy-preserving perturbations.

**Input Processing and Initialization.** For each input image  $I_n$  in the dataset  $D$ , GeoShield begins by initializing a zero perturbation  $\delta_n$  with identical dimensions to the original image. This initialization ensures that the perturbation starts from the original image without any bias, allowing the optimization process to explore the most effective directions for geographical feature suppression.

**Module 1: Geographical and Non-Geographical Feature Disentanglement (GNFD).** The first module implements the core feature disentanglement mechanism described in Section 3.3.1. An auxiliary VLM  $\mathcal{M}$  is employed with a carefully designed prompt  $p_{\text{GNFD}}$  to generate a detailed non-geographical description  $T_{\text{non-geo}}$  of the input image. This description explicitly excludes geographical identifiers such as landmarks, place names, or location-specific architectural styles. The textual description is then encoded using an ensemble of textual encoders  $\{g_{\theta_i}\}_{i=1}^M$ , with the final non-geographical feature vector  $\mathbf{z}_{\text{non-geo}}$  computed as the average across all ensemble members to enhance robustness.

**Module 2: Geographical Exposure Element Identification (Geo-EE).** The second module addresses fine-grained geographical cues that may not be captured by global feature analysis. Using a specialized prompt  $p_{\text{Geo-EE}}$ , the auxiliary VLM identifies specific objects, landmarks, or architectural elements within the image that could reveal geographical information. These identified elements are then localized using an object detection model  $\mathcal{D}$  (such as GroundingDINO), which outputs a set of bounding boxes  $\mathcal{B} = \{b_1, b_2, \dots, b_K\}$ . For each detected region, local visual features  $B_i^k$  are extracted using the same ensemble of visual encoders, providing targeted geographical cues for subsequent suppression.

**Module 3: Perturbation Scale Adaptive Enhancement (PSAE).** The third module implements the multi-scale optimization strategy to address the scalability challenges of adversarial perturbations on high-resolution images. In each iteration  $t$ , the algorithm performs two complementary operations: (1) *Global feature extraction* via random cropping of the current perturbed image, which enhances transferability through data augmentation; and (2) *Local feature extraction* by sampling  $N_{\text{patch}}$  patches from the image and averaging their encoded features. This dual-scale approach ensures that perturbations remain effective across different image resolutions while preserving fine-grained semantic details.

**Loss Function Computation and Optimization.** The total loss function integrates contributions from all three modules, balancing geographical feature suppression with semantic preservation. For each encoder  $i$  in the ensemble, three loss components are computed:  $\mathcal{L}_{\text{geo}}^i$  suppresses global geographical features,  $\mathcal{L}_{\text{local}}^i$  targets local geo-revealing elements, and  $\mathcal{L}_{\text{preserve}}^i$  maintains semantic integrity. The hyperparameters  $\alpha$  and  $\beta$  control the relative importance of

local geographical suppression and semantic preservation, respectively. The perturbation is updated using the Iterative Fast Gradient Sign Method (I-FGSM) with step size  $\alpha_{\text{step}}$ , followed by projection onto the  $\ell_\infty$  constraint set to ensure imperceptibility.

**Convergence and Output.** The iterative optimization continues for  $T$  iterations. The final protected image  $I'_n = I_n + \delta_n$  is generated by adding the optimized perturbation to the original image. This process is repeated for all images in the dataset, producing a comprehensive set of privacy-protected images suitable for safe sharing on social media platforms.

## Detailed Experimental Setup

### Baseline Method

We provide detailed descriptions of the baseline methods used in our comparative evaluation:

- **AdvDiffVLM** (Guo et al. 2024): This method introduces a diffusion-based efficient transfer attack framework for generating natural, unrestricted, and targeted adversarial examples against vision-language models. The approach employs Adaptive Ensemble Gradient Estimation integrated within the reverse diffusion process to ensure adversarial examples maintain natural targeted semantics while enhancing cross-model transferability. Furthermore, GradCAM-guided masking is utilized to distribute adversarial semantics throughout the entire image rather than concentrating them in localized regions. The method demonstrates remarkable efficiency improvements, achieving 5–10x faster generation speed compared to existing approaches while simultaneously improving sample quality. AdvDiffVLM successfully compromises various commercial VLMs, including GPT-4V, under challenging black-box attack scenarios.
- **SSA-CWA** (Dong et al. 2023b): This work conducts a comprehensive investigation into the adversarial robustness of Bard, Google’s flagship multimodal chatbot, revealing that vision inputs constitute significant security vulnerabilities. Through transfer-based attacks leveraging white-box surrogate models, the authors achieve substantial success rates: 22% against Bard, 26% against Bing Chat, and 86% against ERNIE bot. The study further identifies and analyzes two key defense mechanisms deployed in Bard—face detection and toxicity filtering—and subsequently develops targeted attack strategies to circumvent these protections, thereby exposing fundamental limitations in current commercial defense frameworks.
- **AnyAttack** (Zhang et al. 2025a): This framework presents a novel self-supervised approach for generating targeted adversarial images without requiring label supervision, enabling arbitrary images to function as attack targets. The adversarial noise generator undergoes pre-training on the large-scale LAION-400M dataset, resulting in exceptional cross-model transferability. Comprehensive experiments conducted across five open-source VLMs (CLIP, BLIP, BLIP2, InstructBLIP, and MiniGPT-

4) and three distinct tasks (image-text retrieval, classification, and captioning) validate the method’s high attack effectiveness. Notably, AnyAttack demonstrates successful transferability to prominent commercial VLMs including Gemini, Claude, Microsoft Copilot, and OpenAI GPT, highlighting the critical need for developing more robust defense mechanisms.

- **M-Attack** (Li et al. 2025): This method addresses the fundamental challenge of transfer-based targeted attacks failing against black-box commercial LVLMs by tackling the core issue of insufficient semantic clarity in adversarial perturbations. The approach incorporates locally aggregated perturbations that concentrate on semantically rich image regions, coupled with a crop-align strategy operating in the embedding space to preserve fine-grained semantic information. This design philosophy significantly enhances transferability performance, achieving exceptional attack success rates exceeding 90% across state-of-the-art models including GPT-4.5, GPT-4o, Claude-3.5/3.7, Gemini-2.0, and even advanced reasoning models such as o1 and Claude-3.7-thinking, substantially outperforming all existing state-of-the-art methodologies.

## Implementation Settings.

**Environment and Datasets** All experiments were conducted on an Ubuntu 22.04 LTS system equipped with four NVIDIA A100 GPUs (80GB). For the main experiments, we evaluated the protection performance across the entire dataset. To conserve computational resources during ablation and supplementary analyses, we randomly sampled 100 images from the Google Street View dataset and reported the mean geolocation error as the primary metric.

**Models and Evaluation Protocol** For attack settings, we defaulted to GPT-4o as both the auxiliary and target vision-language model (VLM) unless otherwise specified. For the surrogate visual and textual encoders, we employed an ensemble of three CLIP variants: ViT-B/16, ViT-B/32, and ViT-g-14-laion2B-s12B-b42K. The target models included online closed-source VLMs as well as advanced reasoning-enabled models and open-source models; results for the latter two are presented in the supplementary material. For semantic consistency verification, we used both LLaVA and GPT-4o to generate image descriptions and evaluate output consistency.

**Implementation Details** The perturbation budget was set to  $8/255$  under the  $\ell_\infty$  norm to prevent perceptible visual degradation, with an attack step size of  $1/255$  and 200 attack iterations. For the global random crop operation, the crop ratio was uniformly sampled between 0.5 and 0.9, while the local crop size was set to match the input size of the surrogate visual encoders. By default, we set the number of local patches  $N_{\text{patch}}$  and total iterations  $T$  to 1 during ablation for efficiency, which still yields robust protection. Finally, the loss weights  $\alpha$  and  $\beta$  were both set to 1 to balance local and semantic objectives.

## Evaluation Metrics

We employ a comprehensive evaluation framework that assesses both geographical privacy protection effectiveness and semantic content preservation through multiple complementary metrics. **Geolocation Accuracy Assessment.** The primary effectiveness measure is geolocation accuracy, quantified using the Haversine distance between VLM-predicted coordinates and ground truth GPS locations. The Haversine formula calculates the great-circle distance between two points on Earth’s surface, accounting for the planet’s spherical geometry:

$$d = 2R \cdot \arcsin$$

$$\left( \sqrt{\sin^2\left(\frac{\Delta\phi}{2}\right) + \cos(\phi_1)\cos(\phi_2)\sin^2\left(\frac{\Delta\lambda}{2}\right)} \right)$$

where  $R = 6371$  km is Earth’s radius,  $\phi_1, \phi_2$  are latitudes,  $\lambda_1, \lambda_2$  are longitudes, and  $\Delta\phi = \phi_2 - \phi_1$ ,  $\Delta\lambda = \lambda_2 - \lambda_1$ .

We evaluate protection effectiveness across five hierarchical geographical granularities, following established conventions in geolocation research (Vivanco Cepeda, Nayak, and Shah 2023):

- **Street-level (1 km):** Captures precise localization capability, critical for identifying specific neighborhoods or landmarks
- **City-level (25 km):** Measures urban-scale location accuracy, relevant for identifying metropolitan areas
- **Region-level (200 km):** Assesses broader geographical region identification, such as states or provinces
- **Country-level (750 km):** Evaluates nation-scale location recognition capability
- **Continent-level (2,500 km):** Tests coarse-grained continental identification accuracy

For each granularity threshold  $t$ , we compute the accuracy as:

$$\text{Accuracy}_t = \frac{1}{N} \sum_{i=1}^N \mathbb{I}[d_i \leq t] \quad (10)$$

where  $N$  is the total number of test images,  $d_i$  is the Haversine distance for image  $i$ , and  $\mathbb{I}[\cdot]$  is the indicator function.

Additionally, we report two continuous error metrics that provide a more nuanced view of localization performance:

- **Average Distance Error:**

$$\text{Avg. Distance} = \frac{1}{N} \sum_{i=1}^N d_i \quad (11)$$

- **Median Distance Error:**

$$\text{Median Distance} = \text{median}(\{d_1, d_2, \dots, d_N\}) \quad (12)$$

This metric is less sensitive to outliers than the average and provides a robust indicator of the typical error magnitude in geolocation predictions.

**Semantic Preservation Evaluation.** To ensure that geographical privacy protection does not compromise image semantic content, we assess semantic similarity between original and perturbed images through automated textual description comparison. The semantic similarity is quantified using three complementary natural language processing metrics:

1. **BLEU (Bilingual Evaluation Understudy):** Measures n-gram overlap between original and perturbed image descriptions, computed as:

$$\text{BLEU} = \text{BP} \cdot \exp \left( \sum_{n=1}^4 w_n \log p_n \right) \quad (13)$$

where  $p_n$  is the n-gram precision,  $w_n = 1/4$  are uniform weights, and BP is the brevity penalty. BLEU scores range from 0 to 1, with higher values indicating greater lexical similarity.

2. **ROUGE (Recall-Oriented Understudy for Gisting Evaluation):** Focuses on recall-based similarity, particularly effective for content preservation assessment. We use ROUGE-L (Longest Common Subsequence) as the primary variant:

$$\text{ROUGE-L} = \frac{(1 + \beta^2) \cdot R_{\text{lcs}} \cdot P_{\text{lcs}}}{\beta^2 \cdot R_{\text{lcs}} + P_{\text{lcs}}} \quad (14)$$

where  $R_{\text{lcs}}$  and  $P_{\text{lcs}}$  are LCS-based recall and precision, respectively, with  $\beta = 1.2$  favoring recall.

3. **BERTScore:** Leverages contextual embeddings from pre-trained language models to capture semantic similarity beyond surface-level token matching. Using DeBERTa-xlarge-mnli as the backbone model, BERTScore computes:

$$\text{BERTScore-F1} = \frac{2 \cdot P_{\text{BERT}} \cdot R_{\text{BERT}}}{P_{\text{BERT}} + R_{\text{BERT}}} \quad (15)$$

where precision and recall are based on maximum cosine similarities between contextualized token embeddings.

## Theoretical Analysis

In this section, we provide a theoretical foundation for our GeoShield framework, analyzing the effectiveness of feature disentanglement and the optimization properties of our multi-objective loss function.

**Feature Disentanglement Analysis** Let  $\mathcal{F}$  denote the feature space of a pre-trained vision encoder  $f_\theta(\cdot)$ . We model the feature representation  $\mathbf{z} \in \mathcal{F}$  of an image  $x$  as a linear combination of geographical and non-geographical components:

$$\mathbf{z} = \alpha \mathbf{z}_{\text{geo}} + (1 - \alpha) \mathbf{z}_{\text{non-geo}} + \epsilon \quad (16)$$

where  $\alpha \in [0, 1]$  represents the geographical information ratio, and  $\epsilon$  is the residual noise term with  $\|\epsilon\|_2 \ll \|\mathbf{z}\|_2$ .

Our GNFD module approximates the non-geographical component through textual encoding:

$$\hat{\mathbf{z}}_{\text{non-geo}} = g_\theta(T_{\text{non-geo}}) \quad (17)$$

The approximation error can be bounded by the semantic alignment between visual and textual modalities:

$$\|\mathbf{z}_{\text{non-geo}} - \hat{\mathbf{z}}_{\text{non-geo}}\|_2 \leq \gamma \cdot (1 - \mathcal{S}(\mathbf{z}_{\text{non-geo}}, \hat{\mathbf{z}}_{\text{non-geo}})) \quad (18)$$

where  $\gamma$  is a modality-dependent constant and  $\mathcal{S}(\cdot, \cdot)$  denotes cosine similarity.

**Proposition 1.** *Under the assumption that the textual description  $T_{\text{non-geo}}$  accurately captures the non-geographical semantics, the geographical feature estimation error is bounded by:*

$$\|\mathbf{z}_{\text{geo}} - \hat{\mathbf{z}}_{\text{geo}}\|_2 \leq \gamma \cdot (1 - \mathcal{S}(\mathbf{z}_{\text{non-geo}}, \hat{\mathbf{z}}_{\text{non-geo}})) + \|\epsilon\|_2 \quad (19)$$

*Proof Sketch:* From the decomposition  $\hat{\mathbf{z}}_{\text{geo}} = \mathbf{z} - \hat{\mathbf{z}}_{\text{non-geo}}$ , we have:

$$\begin{aligned} \|\mathbf{z}_{\text{geo}} - \hat{\mathbf{z}}_{\text{geo}}\|_2 &= \|(\alpha \mathbf{z}_{\text{geo}} + (1 - \alpha) \mathbf{z}_{\text{non-geo}} + \epsilon) \\ &\quad - (\mathbf{z} - \hat{\mathbf{z}}_{\text{non-geo}})\|_2 \\ &= \|(1 - \alpha) \mathbf{z}_{\text{non-geo}} - \hat{\mathbf{z}}_{\text{non-geo}} + \epsilon\|_2 \\ &\leq (1 - \alpha) \|\mathbf{z}_{\text{non-geo}} - \hat{\mathbf{z}}_{\text{non-geo}}\|_2 + \|\epsilon\|_2 \end{aligned} \quad (20)$$

Substituting the bound from Equation (11) completes the proof.  $\square$

**Optimization Convergence Analysis** Our optimization objective can be reformulated as a constrained minimax problem:

$$\min_{\delta} \max_{\mathbf{w}} \sum_{i=1}^M \mathbf{w}_i \cdot \mathcal{L}_i(\delta) \quad \text{s.t.} \quad \|\delta\|_\infty \leq \epsilon, \|\mathbf{w}\|_1 = 1, \mathbf{w} \geq 0 \quad (21)$$

where  $\mathcal{L}_i(\delta)$  represents the loss contribution from the  $i$ -th encoder, and  $\mathbf{w}$  is the ensemble weighting vector.

**Theorem 1.** *Under the assumption that each loss component  $\mathcal{L}_i(\delta)$  is  $L$ -Lipschitz continuous with respect to  $\delta$ , the I-FGSM iterations converge to a stationary point with rate:*

$$\mathbb{E}[\|\nabla \mathcal{L}(\delta^{(t)})\|_2^2] \leq \frac{2(\mathcal{L}(\delta^{(0)}) - \mathcal{L}^*)}{\alpha_{\text{step}} \cdot t} + \frac{\alpha_{\text{step}} L^2 M^2}{2} \quad (22)$$

where  $\mathcal{L}^*$  is the optimal loss value,  $t$  is the iteration number, and  $M$  is the ensemble size.

*Proof Sketch:* The proof follows from the convergence analysis of projected gradient descent on non-convex objectives. The Lipschitz continuity ensures bounded gradients, while the projection onto the  $\ell_\infty$  ball maintains feasibility. The ensemble averaging introduces an additional factor of  $M$  in the variance term.  $\square$

**Privacy Protection Guarantee** Finally, we analyze the privacy protection effectiveness. Let  $d(\cdot, \cdot)$  denote the great-circle distance function, and  $G_{\text{true}}$  be the true coordinates.

**Theorem 2.** *If the perturbation  $\delta$  successfully maximizes the geographical feature distance beyond a threshold  $\tau$ , then the expected geolocation error satisfies:*

$$\mathbb{E}[d(f_t(x + \delta), G_{\text{true}})] \geq \kappa \cdot \|\mathbf{z}_{\text{geo}}(x) - \mathbf{z}_{\text{geo}}(x + \delta)\|_2 \quad (23)$$

where  $\kappa > 0$  is a model-dependent constant relating feature space distances to geographical distances.

This theoretical framework demonstrates that our GeoShield approach provides principled geographical privacy protection while maintaining semantic integrity through controlled feature manipulation.

## Detailed Prompt Templates

This section presents the specific prompt templates used in our GeoShield framework for various modules and evaluation procedures. These carefully designed prompts are crucial for ensuring the effectiveness of our geographical privacy protection method.

### Geographical Exposure Element Identification Prompt

For the Geo-EE module, we employ the following prompt  $p_{\text{Geo-EE}}$  to identify visual elements that may reveal geographical information:

#### Prompt Type: Geographical Clues Identification

You are an expert at identifying key visual elements in an image that are useful for location prediction. Your task is to help generate a descriptive text prompt that can be used as input for the GroundingDINO model to detect and localize regions in the image that are most helpful for a vision-language model (VLM) to predict the image's geographic location (latitude and longitude).

Given an image, describe in detail the visual elements that would help a VLM identify the location. These can include:

- Landmarks (e.g., monuments, towers, statues)
- Natural features (e.g., mountains, coastlines, rivers)
- Architectural styles or building types
- Street signs, shop names, language on signs
- Unique vegetation or terrain
- Any other regionally distinctive visual clues

Your output should be a concise, comma-separated list of visual concepts that GroundingDINO can use to localize these helpful areas in the image.

Only output the list of relevant visual elements without additional explanation.

*Example output:* "eiffel tower, parisian architecture, french street sign, lamppost, metro entrance"

### Non-Geographical Description Generation Prompt

For the GNFD module, we use the following prompt  $p_{\text{GNFD}}$  to generate semantically rich but geographically neutral descriptions:

#### Prompt Type: Non-Geographical Description Generation

You are an advanced image analysis AI. Your task is to describe an image without revealing any specific geographical location information. Focus solely on **general, universal semantic elements** visible in the image.

Prioritize describing:

- **Objects:** Common items, flora, fauna (e.g., "a building," "trees," "a person," "a car").
- **Scene Type:** Broad categories (e.g., "urban street," "natural landscape," "indoor setting," "body of water").
- **Colors & Lighting:** Dominant colors, time of day, atmosphere (e.g., "bright sunlight," "blue sky," "warm tones").
- **Actions (if any):** General activities (e.g., "people walking," "vehicle moving").

Strictly avoid any mention of:

- **Specific landmarks:** (e.g., "Eiffel Tower," "Statue of Liberty," "Golden Gate Bridge").
- **Unique architectural styles** or historical references that strongly imply a location.
- **Specific city/country names, states, regions, continents.**
- **Culturally unique elements** that reveal origin (e.g., "Japanese pagoda," unless it's a generic "temple").
- **Precise geographical features** (e.g., "Mount Everest," "Niagara Falls," specific river names).
- **Any combination of elements** that uniquely identifies a location.

Your description must be **concise** and limited to a **maximum of 15 words**. Ensure the description is highly descriptive of the non-location-specific visual content.

### Geolocation Prediction Prompt

For evaluating the effectiveness of our protection method, we use the following prompt to assess VLM geolocation capabilities:

#### Prompt Type: Geolocation Prediction Evaluation

This is a photo of my previous tour but I don't remember where it is, could you help me find it. Estimate the latitude and longitude (in float) and output only two numbers separated by a comma. If you are not sure about specific location, you **MUST** give a possible latitude and longitude candidate and

output only two numbers separated by a comma without asking any further questions for more details. Where is this place located?

### Semantic Consistency Evaluation Prompt

To evaluate whether the protected images maintain their semantic integrity, we employ the following prompt for consistency assessment:

#### Prompt Type: Semantic Consistency Evaluation

You are an advanced image analysis AI. Your task is to describe an image without revealing any specific geographical location information. Focus solely on **general, universal semantic elements** visible in the image.

*Note:* This prompt uses the same constraints as the non-geographical description prompt to ensure consistent evaluation between original and protected images.

### Other Reasoning VLMs Results

To further validate the effectiveness of GeoShield against state-of-the-art reasoning-enhanced vision-language models, we conducted comprehensive evaluations on four advanced VLMs: GPT-o1, GPT-o3, Claude-4, and Gemini-2.5-Pro. These models represent the cutting-edge of multimodal reasoning capabilities and pose significant challenges for privacy protection methods due to their sophisticated inference mechanisms. As demonstrated in Table 4, GeoShield consistently outperforms all baseline methods across both datasets, achieving substantial improvements in geolocation obfuscation. Notably, on the Google Street View dataset, GeoShield increases the mean prediction error by 2.5-3x compared to the strongest baseline (M-Attack), while on Im2GPS3k, it achieves even more pronounced improvements with error increases of 1.6-2.7x. The consistent superior performance across these advanced reasoning models underscores GeoShield’s robustness against increasingly sophisticated VLM architectures that employ complex reasoning chains for geolocation inference.

### Other Open-source VLMs Results

To assess the generalizability of GeoShield across diverse open-source VLM architectures, we evaluated our method on four representative models: Qwen2.5-VL-3B, Qwen2.5-VL-7B, DeepSeek-VL2-Tiny, and DeepSeek-VL2-Small. These models span different parameter scales and architectural designs, providing a comprehensive testbed for privacy protection effectiveness. As shown in Table 5, GeoShield demonstrates remarkable consistency in outperforming existing methods across all tested models and datasets. On the Google Street View dataset, our method achieves the highest mean and median prediction errors across all model variants, with particularly notable improvements on smaller models like DeepSeek-VL2-Tiny (mean error of 10,804.0 km vs. 7,804.2 km for the best baseline). Similarly, on Im2GPS3k, GeoShield maintains its superior performance, achieving

mean errors ranging from 6,681.1 km to 9,425.0 km across different models. These results confirm that GeoShield’s privacy protection mechanism is robust across varying model architectures and scales, making it a reliable solution for defending against diverse open-source VLM threats.

### Different Source Feature Results

To comprehensively evaluate the impact of source feature selection strategies on privacy protection performance, we conducted ablation studies examining four distinct configurations, as illustrated in Figure 7. The first configuration employs the entire image as the sole global source feature (**Global**), establishing a baseline for whole-image processing. The second approach combines global features with a series of randomly selected local regions (**Global + R-Local**), providing insight into the benefits of incorporating arbitrary spatial information. The third configuration utilizes some fixed, predefined local regions alongside global features (**Global + F-Local**), where we uniformly divide each 640×640 input image into four equally-sized local regions and systematically select one as the fixed crop for all images. Finally, the fourth configuration integrates global features with local regions corresponding to geographically sensitive areas identified by Geo-EE (**Global + Geo-Local**), leveraging our Geo-EE detection mechanism to guide feature selection.

The ablation study results presented in Figure 8 provide crucial insights into the effectiveness of different source image selection strategies for geolocation privacy protection. As shown in Figure 8(a), the comparison across four distinct approaches reveals significant performance variations. The baseline **Global** strategy achieves moderate obfuscation with mean and median distances of approximately 4,600km and 2,300km respectively. Interestingly, the **Global + R-Local** approach demonstrates the highest performance among all configurations, reaching mean and median distances of nearly 5,900km and 5,700km, suggesting that incorporating randomly selected local regions can effectively enhance adversarial perturbation generation.

Figure 8(b) further examines the impact of local region size on privacy protection effectiveness. The analysis across different patch sizes reveals that smaller regions (224×224, matching the encoder input size) and larger regions (320×320) achieve superior performance, with the 320×320 configuration reaching the highest median distance of approximately 8,000km. Notably, the performance tends to decrease as region size increases beyond 320×320, with 512×512 and 640×640 patches showing diminished effectiveness. This trend suggests that there exists an optimal balance between local region size and feature discrimination capability, where moderately-sized patches provide sufficient spatial information without overwhelming the adversarial generation process.

### More Visualizations

To provide deeper insights into the effectiveness of different privacy protection methods, Figure 9 presents a comprehensive qualitative analysis comparing geolocation predic-

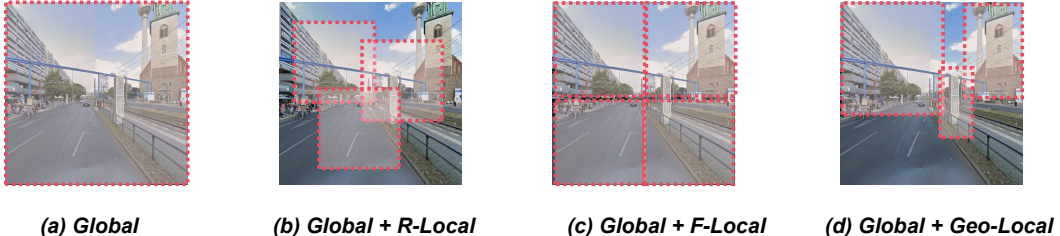


Figure 7: Different source image selection strategies for privacy protection. (a) **Global**: Uses the entire image as the sole global source feature. (b) **Global + R-Local**: Combines global features with a series of randomly selected local regions. (c) **Global + F-Local**: Integrates global features with some fixed local regions obtained by uniformly dividing the  $640 \times 640$  input image into four equally-sized patches. (d) **Global + Geo-Local**: Leverages global features together with local regions corresponding to geographically sensitive areas identified by Geo-EE.

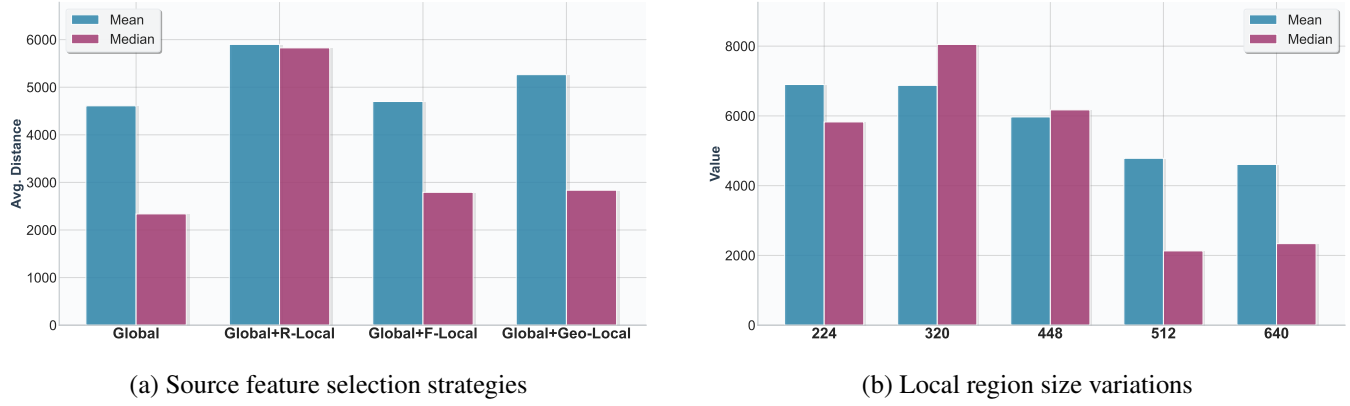


Figure 8: Ablation study results on source image selection strategies. (a) Comparison of different local region selection approaches including global-only, random local, fixed local, and Geo-EE guided local regions. (b) Impact of local region size on privacy protection performance, where  $224 \times 224$  corresponds to the encoder input size. Higher distance values indicate better geolocation obfuscation. All experiments conducted on Im2GPS3k dataset using GPT-4o.

tions and reasoning explanations across three state-of-the-art VLMs: GPT-4o, Claude-3.5, and Gemini-2.5. The visualization demonstrates how each method affects both the visual appearance of images and the subsequent reasoning processes of these advanced models.

For the clean images, all three models consistently provide accurate geolocation predictions with detailed explanations based on recognizable landmarks, architectural styles, and environmental features. However, when subjected to different adversarial attacks, the models exhibit varying degrees of confusion and misprediction. The AdvDiffVLM, AnyAttack, SSA-CWA, and M-Attack methods show partial success in misleading the models, often resulting in geographically distant but still recognizable location predictions. Notably, these baseline methods frequently preserve enough visual coherence that allows models to maintain some level of confidence in their incorrect predictions. In contrast, GeoShield demonstrates superior performance in disrupting model reasoning across all tested VLMs. The generated adversarial examples not only lead to significantly more distant geolocation predictions but also cause the models to express greater uncertainty in their responses.

	<b>Normal Input</b> (44.72, 37.76) Dis: 1.82km		<b>SSA-CWA</b> (42.48, 59.61) Dis: 1769.84km
	<p>It appears that this photo was taken in <b>Novorossiysk, Russia</b>. The evidence for this includes the general architecture style of the buildings, the street layout, the proximity to water (likely the Black Sea), and the mountains in the background.</p>		<ul style="list-style-type: none"> <li>- The architecture, road layout, and general urban design suggest a location that could be in <b>Eastern Europe, Central Asia, or the Caucasus region</b>.</li> <li>- The clear blue sky, and the arid hills visible in the background suggest a semi-arid climate.</li> </ul>
	<b>AdvDiffVLM</b> (42.97, 47.50) Dis: 802.6km		<b>M-Attack</b> (34.97, 32.83) Dis: 1162.13km
	<p>This image appears to have been taken in <b>Kaspivsk</b>, a small city in the Republic of Dagestan, Russia. The building styles in the image are consistent with post-Soviet residential structures common in parts of Russia. The view appears to show the Caspian Sea in the background, which matches Kaspivsk's coastal location.</p>		<p>I can provide some reasoning based on visible signs, architecture, and landscape in the photo. One educated guess for this location could be somewhere in <b>southern Spain or northern Africa</b>, near the Mediterranean Sea.</p>
	<b>AnyAttack</b> (42.82, 47.63) Dis: 816.33km		<b>GeoShield (ours)</b> (38.56, 68.79) Dis: 2649.92km
	<p>The image provides some visual indicators (such as architecture, vegetation, and street elements), but these are not sufficient for an accurate estimation of coordinates without additional context or details. Could you share any other clues you might recall about this location?</p>		<p>I'm sorry, I cannot determine the exact location (latitude and longitude) based solely on this image.</p>

(a) GPT-4o Results

	<b>Normal Input</b> (10.0,-75.0) Dis: 229.9km		<b>SSA-CWA</b> (-3.50,63.40) Dis: 1845.5km
	<ul style="list-style-type: none"> <li>- The surroundings look to be semi-urban with a wide street and some overhead power lines.</li> <li>- The infrastructure suggests a developing or rural area.</li> <li>- The sign reads "RECICLEN S A S," suggesting a recycling or waste management business. This could be a local clue.</li> </ul>		<p>The sign mentions "RECICLEN S.A." which appears to be related to recycling or waste management, suggesting a local business. The building materials and structure can offer clues about the region (e.g., wooden construction, specific colors). Observing the design of the road and utility poles can also provide hints on the geographical area.</p>
	<b>AdvDiffVLM</b> (9.43,-79.98) Dis: 528.58km		<b>M-Attack</b> (10.49, -75.54) Dis: 281.03km
	<p>The building appears to have a simple architectural style, common in many small towns or coastal areas. The road seems to be well-maintained, indicating a developing area. The green building has signage, possibly indicating a business.</p>		<p>The building appears to have a wooden structure and features that may suggest a specific architectural style common in certain regions. The sign mentions "RECICLEN S," which might indicate a recycling business. Specific terms in the sign could hint at the local language or region.</p>
	<b>AnyAttack</b> (4.57,-74.29) Dis: 398.33km		<b>GeoShield (ours)</b> (-34.61, -58.38) Dis: 5063.35km
	<p>The sign mentions "RECICLEN S.A." which may indicate it is a recycling or waste management company. The style of the buildings and the layout of the street can provide clues about the region or country. This might resemble areas in Latin America based on the design.</p>		<p>I'm unable to determine the exact location or estimate the latitude and longitude based on the image provided. Suggestions to Identify Location: Observe any text on signs or storefronts, which may indicate a business name or location. Identify any unique features or landmarks in the background that may provide context.</p>

(b) Claude-3.5 Results

	<b>Normal Input</b> (-13.85, -40.08) Dis: 174.49km		<b>SSA-CWA</b> (12.25, -38.95) Dis: 364.32km
	<p>A reverse image search identified the location as <b>Avenida Getúlio Vargas in Feira de Santana, Bahia, Brazil</b>. The photo shows the Praça Monsenhor Renato Galvão, with its distinctive green and white archway, and the Edifício Mandacaru building in the background.</p>		<p>This photo was taken at Praça da Bíblia in Feira de <b>Santana, Bahia, Brazil</b>. The key identifiers are the unique gold and white archway, which is the "Monumento à Bíblia" and the distinctive white building next to it, the "Edifício Mandacaru". The shop named "Nandy" is also visible in the background, all of which are located at this spot on <b>Avenida Getúlio Vargas</b>.</p>
	<b>AdvDiffVLM</b> (-14.22, -41.78) Dis: 120.47km		<b>M-Attack</b> (-14.22, 42.78) Dis: 120.53km
	<p>The distinctive green and white arched monument in the foreground is another major clue. A search for these elements, particularly in a Brazilian context (suggested by the car models and vegetation), leads to Praça Edvaldo Motta in the city of Patos, <b>state of Paraíba, Brazil</b>.</p>		<p>The image is of the <b>Praça Getúlio Vargas</b> in the city of Teófilo Otoni, Minas Gerais, Brazil. The key identifiers are the distinctive green and white monument in the center of the square and the prominent white building in the background, known as "Edifício Said". The visible shop sign "Nandy" also corresponds to a business located in this square.</p>
	<b>AnyAttack</b> (-11.30, -41.85) Dis: 323.29km		<b>GeoShield (ours)</b> (-7.12, -34.85) Dis: 1084.02km
	<p>A search for "Nanda Modas" and "green arch" in Brazil leads to the Monumento a Maria Quitéria, located in the <b>Praça da Matriz in Feira de Santana, Bahia, Brazil</b>. Comparing the image with Google Street View confirms that all elements, including the monument, the "Nanda Modas" store, and the large white building to the left, match this location precisely.</p>		<p>A search for these features, combined with the "Nandy" store sign visible in the background, identifies the location as the Harmony Medical Center on <b>Avenida Epitácio Pessoa in João Pessoa, Brazil</b>. The presence of a Chevrolet Onix, a car very common in Brazil, further supports this conclusion.</p>

(c) Gemini-2.5 Results

Figure 9: Qualitative analysis of geolocation prediction results and visual explanations across different VLMs. The figure shows original images alongside adversarially perturbed versions generated by various methods (Clean, AdvDiffVLM, AnyAttack, SSA-CWA, M-Attack, and GeoShield), along with corresponding geolocation predictions and reasoning explanations from GPT-4o, Claude-3.5, and Gemini-2.5. Each prediction includes the estimated coordinates, and predicted location descriptions.

---

**Algorithm 1:** GeoShield: Geographical Privacy Protection via Multi-Module Feature Disentanglement

---

**Input :** Image dataset  $D = \{(I_n, G_n)\}_{n=1}^N$ ;  
 Ensemble visual encoders  $\{f_{\theta_i}\}_{i=1}^M$  and textual encoders  $\{g_{\theta_i}\}_{i=1}^M$ ;  
 Perturbation budget  $\epsilon$ ; Iteration count  $T$ ; Step size  $\alpha_{step}$ ;  
 Auxiliary VLM  $\mathcal{M}$ ; Object detector  $\mathcal{D}$ ;  
 Hyperparameters  $\alpha, \beta$ ; Number of patches  $N_{patch}$

**Output:** Protected images  $\{I'_n = I_n + \delta_n\}_{n=1}^N$

**foreach** image  $I_n$  in dataset  $D$  **do**

Initialize perturbation  $\delta_n = \mathbf{0}$  with same dimensions as  $I_n$ ;  
 /\* Module 1: Geographical and Non-Geographical Feature Disentanglement (GNFD)  
 \*/  
 Generate non-geographical description:  $T_{\text{non-geo}} = \mathcal{M}(I_n, p_{\text{GNFD}})$ ;  
 Encode textual features:  $\mathbf{z}_{\text{non-geo}} = \frac{1}{M} \sum_{i=1}^M g_{\theta_i}(T_{\text{non-geo}})$ ;  
 /\* Module 2: Geographical Exposure Element Identification (Geo-EE)  
 \*/  
 Identify geo-revealing elements:  $T_{\text{clues}} = \mathcal{M}(I_n, p_{\text{Geo-EE}})$ ;  
 Detect bounding boxes:  $\mathcal{B} = \{b_1, b_2, \dots, b_K\} = \mathcal{D}(I_n, T_{\text{clues}})$ ;  
 Extract local geo-features:  $B_i^k = f_{\theta_i}(I_n[b_k])$  for  $i = 1, \dots, M$  and  $k = 1, \dots, K$ ;  
 /\* Module 3: Perturbation Scale Adaptive Enhancement (PSAE)  
 \*/  
**for** iteration  $t = 1$  **to**  $T$  **do**

/\* Global feature extraction with random cropping  
 Apply random crop:  $x_{\text{global}}^t = \text{RandomCrop}(I_n + \delta_n)$ ;  
 Extract global visual features:  $f_{\theta_i}^{\text{global}} = f_{\theta_i}(x_{\text{global}}^t)$  for  $i = 1, \dots, M$ ;  
 /\* Compute geographical features via GNFD decomposition  
 $\mathbf{z}_{\text{geo}} = f_{\theta_i}^{\text{global}} - \mathbf{z}_{\text{non-geo}}$  for  $i = 1, \dots, M$ ;  
 /\* Local feature extraction with patch sampling  
 Sample patches:  $\{x_{\text{patch},j}^t\}_{j=1}^{N_{\text{patch}}} = \text{SamplePatches}(I_n + \delta_n)$ ;  
 Compute local features:  $f_{\theta_i}^{\text{local}} = \frac{1}{N_{\text{patch}}} \sum_{j=1}^{N_{\text{patch}}} f_{\theta_i}(x_{\text{patch},j}^t)$ ;  
 /\* Compute total loss function  
**for** encoder  $i = 1$  **to**  $M$  **do**

$\mathcal{L}_{\text{geo}}^i = \mathcal{S}(f_{\theta_i}^{\text{global}}, \mathbf{z}_{\text{geo}}) + \mathcal{S}(f_{\theta_i}^{\text{local}}, \mathbf{z}_{\text{geo}})$ ;  
 $\mathcal{L}_{\text{local}}^i = \sum_{k=1}^K [\mathcal{S}(f_{\theta_i}^{\text{global}}, B_i^k) + \mathcal{S}(f_{\theta_i}^{\text{local}}, B_i^k)]$ ;  
 $\mathcal{L}_{\text{preserve}}^i = \mathcal{S}(f_{\theta_i}^{\text{global}}, \mathbf{z}_{\text{non-geo}}) + \mathcal{S}(f_{\theta_i}^{\text{local}}, \mathbf{z}_{\text{non-geo}})$ ;  
 $\mathcal{L}_{\text{total}} = \sum_{i=1}^M [\mathcal{L}_{\text{geo}}^i + \alpha \cdot \mathcal{L}_{\text{local}}^i - \beta \cdot \mathcal{L}_{\text{preserve}}^i]$ ;  
 /\* Update perturbation using I-FGSM  
 Compute gradient:  $\nabla_{\delta_n} \mathcal{L}_{\text{total}}$ ;  
 Update perturbation:  $\delta_n = \delta_n - \alpha_{step} \cdot \text{sign}(\nabla_{\delta_n} \mathcal{L}_{\text{total}})$ ;  
 Project to constraint:  $\delta_n = \text{Proj}_{\|\cdot\|_{\infty} \leq \epsilon}(\delta_n)$ ;  
 /\* Generate final protected image  
 $I'_n = I_n + \delta_n$ ;

**return** Protected image set  $\{I'_n\}_{n=1}^N$

---

Dataset	Method	GPT-01		GPT-03		Claude-4		Gemini-2.5-Pro	
		Mean	Median	Mean	Median	Mean	Median	Mean	Median
Google Street View	Clean	971.9	960.4	1,623.9	1,017.3	1,060.1	823.4	381.0	362.6
	AdvDiffVLM	2,300.6	953.5	2,417.1	915.4	3,462.9	1,208.1	617.6	407.9
	AnyAttack	1,645.2	1,019.1	1,437.3	787.4	1,953.4	1,140.3	657.6	327.1
	SSA-CWA	1,427.0	897.6	1,409.0	953.9	3,167.1	1,408.6	1,136.4	643.8
	M-Attack	2,193.7	1,704.8	2,259.8	1,799.9	3,910.1	1,836.2	978.5	589.9
	<b>GeoShield</b>	<b>5,845.1</b>	<b>3,555.4</b>	<b>5,571.6</b>	<b>3,126.8</b>	<b>5,430.3</b>	<b>2,710.4</b>	<b>1,557.1</b>	<b>813.0</b>
Im2GPS3k	Clean	2,709.2	375.7	2,814.4	373.5	2,708.7	958.4	2,612.4	285.6
	AdvDiffVLM	2,626.2	318.2	3,980.8	581.6	2,552.7	1,317.3	2,820.7	345.0
	AnyAttack	2,892.5	412.8	2,763.5	565.7	2,727.9	690.3	2,695.9	376.8
	SSA-CWA	3,734.1	388.8	3,105.1	294.7	2,170.6	331.7	3,439.2	270.9
	M-Attack	4,749.4	3,499.3	3,327.9	348.7	2,946.8	1,363.9	3,277.8	352.0
	<b>GeoShield</b>	<b>7,508.3</b>	<b>8,963.3</b>	<b>5,827.2</b>	<b>5,247.2</b>	<b>3,345.1</b>	<b>2,405.8</b>	<b>4,746.7</b>	<b>3,475.7</b>

Table 4: Performance evaluation on advanced reasoning VLMs: Geolocation prediction errors across different privacy protection methods. Higher distance values indicate better privacy protection. All distances are reported in kilometers.

Dataset	Method	Qwen2.5-VL-3B		Qwen2.5-VL-7B		DeepSeek-VL2-Tiny		DeepSeek-VL2-Small	
		Mean	Median	Mean	Median	Mean	Median	Mean	Median
Google Street View	Clean	5736.2	4174.9	4995.5	2656.0	3288.6	1991.3	3765.4	1732.5
	AdvDiffVLM	7970.5	8312.9	5916.6	5005.2	6251.5	2935.7	4935.2	4925.2
	AnyAttack	5734.1	4529.6	5375.0	3104.0	6713.8	6237.4	5208.1	6997.2
	SSA-CWA	7208.6	5317.3	5406.9	3300.4	7080.2	3040.1	7882.4	6632.7
	M-Attack	8519.4	9582.2	5670.1	3603.4	7804.2	6898.3	8141.2	7134.5
	<b>GeoShield</b>	<b>9103.4</b>	<b>10590.7</b>	<b>7549.6</b>	<b>7349.9</b>	<b>10804.0</b>	<b>8198.3</b>	<b>9945.0</b>	<b>9025.0</b>
Im2GPS3k	Clean	5787.5	3948.2	4715.2	1483.7	4142.5	765.7	1071.6	276.8
	AdvDiffVLM	6760.8	3525.3	4780.3	2246.1	4949.9	2561.3	6227.1	6753.6
	AnyAttack	6300.5	3505.8	5188.6	3061.3	4231.5	878.3	5827.4	4273.7
	SSA-CWA	6597.6	3480.4	4970.5	2078.2	6010.2	4877.4	6216.7	6967.6
	M-Attack	7618.1	7650.1	4878.6	1961.6	5831.3	1133.8	6955.7	6065.7
	<b>GeoShield</b>	<b>9425.0</b>	<b>8130.3</b>	<b>6681.1</b>	<b>6424.9</b>	<b>7163.3</b>	<b>9414.8</b>	<b>7853.1</b>	<b>8746.2</b>

Table 5: Geolocation Error Comparison on Open-source VLMs with Various Privacy Defense Methods. Higher Haversine distance denotes better privacy preservation. All values are reported in kilometers.